

# SoFAR: Shortcut-based Fractal Architectures for Binary Convolutional Neural Networks

Zhu Baozhou<sup>1</sup>, Peter Hofstee<sup>1,2</sup>, Jinho Lee<sup>3</sup>, Zaid Al-Ars<sup>1</sup>

<sup>1</sup>Delft University of Technology, Delft, Netherlands

<sup>2</sup>IBM Research Austin, TX, USA

<sup>3</sup>Yonsei University, Seoul, Korea

## Abstract

Binary Convolutional Neural Networks (BCNNs) can significantly improve the efficiency of Deep Convolutional Neural Networks (DCNNs) for their deployment on resource-constrained platforms, such as mobile and embedded systems. However, the accuracy degradation of BCNNs is still considerable compared with their full precision counterpart, impeding their practical deployment. Because of the inevitable binarization error in the forward propagation and gradient mismatch problem in the backward propagation, it is nontrivial to train BCNNs to achieve satisfactory accuracy. To ease the difficulty of training, the shortcut-based BCNNs, such as residual connection-based Bi-real ResNet and dense connection-based BinaryDenseNet, introduce additional shortcuts in addition to the shortcuts already present in their full precision counterparts. Furthermore, fractal architectures have been also been used to improve the training process of full-precision DCNNs since the fractal structure triggers effects akin to deep supervision and lateral student-teacher information flow. Inspired by the shortcuts and fractal architectures, we propose two Shortcut-based Fractal Architectures (SoFAR) specifically designed for BCNNs: 1. residual connection-based fractal architectures for binary ResNet, and 2. dense connection-based fractal architectures for binary DenseNet. Our proposed SoFAR combines the adoption of shortcuts and the fractal architectures in one unified model, which is helpful in the training of BCNNs. Results show that our proposed SoFAR achieves better accuracy compared with shortcut-based BCNNs. Specifically, the Top-1 accuracy of our proposed RF-c4d8 ResNet37(41) and DRF-c2d2 DenseNet51(53) on ImageNet outperforms Bi-real ResNet18(64) and BinaryDenseNet51(32) by 3.29% and 1.41%, respectively, with the same computational complexity overhead.

## Introduction

Convolutional Neural Networks (CNNs) have become the paradigm of choice for visual recognition and made considerable breakthroughs in a wide range of visual tasks (Khan et al. 2020), such as image recognition (He et al. 2016; Verelst and Tuytelaars 2020), object detection (Liu et al. 2020), and segmentation (Chen et al. 2017). To practically deploy CNNs in the field, their efficiency has become a key differentiator, especially when targeting resource-limited embedded platforms.

A significant amount research has been dedicated to increasing the efficiency of CNNs, including pruning (He et al. 2020; Wang et al. 2020), quantization (Cai et al. 2020), knowledge distillation (Romero et al. 2014; Li et al. 2020a), and efficient network design (Howard et al. 2019). In low bit-width quantization, fixed-point integers are used instead of floating-point numbers (Zhou et al. 2016), where binarization is an extreme case of quantization. In BCNNs, the weights and/or activations are represented with only one bit, so the computation of the binary convolution can be completed by XNOR and Popcount bitwise operations (Rastegari et al. 2016). Binarization is the most efficient among the different bit-widths quantization methods, however, it results in accuracy degradation that is too large to be deployed in practice.

The current methods to improve the accuracy of binarization can be divided into two categories (Zhuang et al. 2019): value approximation and structure approximation. In value approximation, we preserve the topology of the full-precision CNNs during the binarization and seek a better local minimum for binarized weights/activations by either minimizing the quantization error (Mishra et al. 2017; Shen et al. 2019; Martinez et al. 2020; Bulat and Tzimiropoulos 2019; Zhu, Al-Ars, and Pan 2020), improving the loss function of the network (Wang et al. 2019; Ding et al. 2019; Mishra and Marr 2017; Hou, Yao, and Kwok 2016), or improving the quantization functions (Darabi et al. 2018; Liu et al. 2018; Lahoud et al. 2019; Yang et al. 2019; Qin et al. 2020). In structure approximation (Liu et al. 2018; Bethge et al. 2019; Zhu, Al-Ars, and Hofstee 2020; Zhuang et al. 2019), the architecture of the binary CNNs is redesigned to approximate the original full-precision CNNs. The structure approximation focuses on the architecture design principles for efficient and accurate BCNNs, which is complementary to the value approximation. In this paper, our proposed method belongs to the structure approximation category.

Regarding structure approximation, Bi-real ResNet (Liu et al. 2018) and BinaryDenseNet (Bethge et al. 2019) show significant accuracy improvement without increasing the number of parameters, which indicates that adopting more shortcuts can help the training of BCNNs. In fractal architectures (Larsson, Maire, and Shakhnarovich 2016), implicit deep supervision (Lee et al. 2015) and student-teacher behavior (Ba and Caruana 2014) ensure the training of full-

precision DCNNs without shortcuts, which shows the potential advantage of fractal architectures for dealing with the difficulty of training CNNs. Inspired by the shortcuts and fractal architectures, we propose our Shortcut-based Fractal Architectures (SoFAR) for BCNNs, which benefit from both the shortcuts and fractal architectures, and unifies them in one model.

The contribution of this paper is summarized as follows.

- We develop two shortcut-based fractal architectures (SoFAR) for BCNNs: the residual connection-based fractal architectures for binary ResNet and the dense connection-based fractal architectures for binary DenseNet.
- Our proposed SoFAR improves on the accuracy of state-of-the-art shortcut-based BCNNs, achieving a better trade-off between efficiency and accuracy.
- On classification tasks, diverse experiments are conducted to demonstrate the effectiveness of our proposed SoFAR.

### Related work

In this section, we review and compare the recent work of compact architecture design and quantized CNNs.

#### Compact architecture design

Efficient architecture design has attracted lots of attention from researchers.  $3 \times 3$  convolution has been replaced with  $1 \times 1$  convolution in GoogLeNet (Szegedy et al. 2015) and SqueezeNet (Iandola et al. 2016) to reduce the computational complexity. Group convolution (Zhang et al. 2019), depthwise separable convolution (Howard et al. 2019), shuffle operation (Ma et al. 2018), and shift operation (Wu et al. 2018a) are shown to reduce the computational complexity of traditional convolution. Instead of relying on human experts, neural architecture search techniques (Tan et al. 2019; Wu et al. 2019) can automatically provide optimized platform-specific architectures, achieving state-of-the-art efficiency.

#### Quantized Convolutional Neural Networks

Low bit-width quantization has been extensively explored in recent work, including reducing the gradient error (Gong et al. 2019), improving the loss function of the network (Jung et al. 2019), and minimizing the quantization error (He and Fan 2019). Moreover, mixed-precision quantized neural networks are developed to improve the performance further for low bit-width quantized neural networks. Using neural architecture search, mixed-precision neural networks (Wu et al. 2018b; Li et al. 2020b; Dong et al. 2019) are developed to find the optimal bit-width (i.e., precision) for weights and activations of each layer efficiently.

Improving network loss function (Wang et al. 2019), minimizing the quantization error (Martinez et al. 2020), and reducing the gradient error (Qin et al. 2020) have been studied to provide a better value approximation for BCNNs. Channel-wise Interaction based Binary Convolutional Neural Network (CI-BCNN) (Wang et al. 2019) uses a reinforcement learning model to mine the channel-wise interactions and impose channel-wise priors to alleviate the inconsistency of signs in binary feature maps. (Martinez et al. 2020)

obtain significant accuracy gains by minimizing the discrepancy between the output of the binary and the corresponding real-valued convolution. Information Retention Network (IR-Net) (Qin et al. 2020) is proposed to retain the information that consists of the forward activations and backward gradients. Regarding structure approximation, (Liu et al. 2018; Bethge et al. 2019) adopts more shortcuts to help the training of BCNNs, which inspires aspects of our proposal.

### Binarization function

In this section, we describe the binarization function that we adopt for our SoFAR, including the binarization of weights (Rastegari et al. 2016) and activations (Liu et al. 2018). We adopt the straight-through estimator (STE) (Bengio, Léonard, and Courville 2013) to approximate the gradient calculation for  $\text{sign}(\cdot)$  function.

#### Binarization of weights

The forward propagation and backward propagation to binarize the weights are calculated as follows.  $E$  and  $L$  refer to the mean of the absolute value of the weights and the loss of the model, respectively.  $W$  and  $W_b$  represent the full precision weights and binary weights.

$$\begin{aligned} \text{Forward: } W_b &= E \times \text{sign}(W) \\ \text{Backward: } \frac{\partial L}{\partial W} &= \frac{\partial L}{\partial W_b} \times \frac{\partial W_b}{\partial W} \approx E \times \frac{\partial L}{\partial W_b} \end{aligned} \quad (1)$$

#### Binarization of activations

The forward propagation and backward propagation to binarize the activations are calculated as follows.  $A$  and  $A_b$  represent the full precision activations and binary activations, respectively.

$$\begin{aligned} \text{Forward: } A_b &= \text{sign}(A) \\ \text{Backward: } \frac{\partial L}{\partial A} &= \frac{\partial L}{\partial A_b} \times \frac{\partial A_b}{\partial A} \\ \text{where } \frac{\partial A_b}{\partial A} &= \begin{cases} 2 + 2A, & -1 < A < 0 \\ 2 - 2A, & 0 \leq A < 1 \\ 0, & \text{otherwise} \end{cases} \end{aligned} \quad (2)$$

### Shortcut-based fractal architectures

In this section, we introduce our proposed SoFAR for BCNNs. Residual connections in ResNet (He et al. 2016) and dense connections in DenseNet (Huang et al. 2017) are the most widely used shortcuts. Thus, we develop the residual connection-based fractal architectures for binary ResNet and the dense connection-based fractal architectures for binary DenseNet.

#### Fractal architectures

In fractal architectures for CNNs (Larsson, Maire, and Shakhnarovich 2016), the truncated fractal with the index of  $C$  can be defined as  $F_C$ , which can be a convolutional layer or convolutional block consisting of several convolutional layers.  $I$  refers to the input activations of the truncated fractal. To have fractal architectures for CNNs, we have to

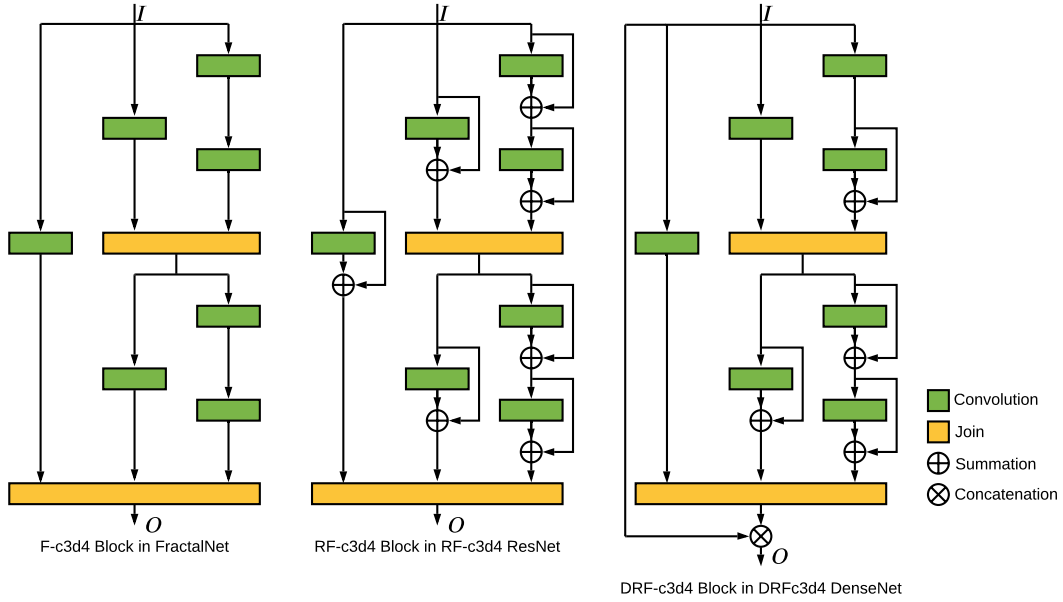


Figure 1: The diagrams of fractal architectures, residual connection-based fractal architectures, and dense connection-based fractal architectures. Blocks in yellow and green refer to join and convolutional layers, respectively.  $\oplus$  and  $\otimes$  refer to feature aggregation of summation and concatenation, respectively.

define the base case and iteration rule. We use a single convolutional layer as the base case of the fractal architectures and define the successive fractals recursively as follows.

$$\begin{aligned} F_1(I) &= \text{Conv}(I) \\ F_{C+1}(I) &= (F_C \otimes F_C(I)) \odot \text{Conv}(I) \end{aligned} \quad (3)$$

where  $\otimes$  denotes composition operation and  $\odot$  represents the join layer. The join layer is used to calculate the element-wise mean of all the inputs. It is worth noting that the neighboring join layers are collapsed into one single join layer as we expand the fractal architectures. The F-c3d4 block is shown to the left of Figure 1, where the Batch Normalization and ReLU layers are omitted.  $c3$  means that the number of columns of the fractal block is  $c = 3$ . Similarly,  $d4$  indicates that the longest depth between the input and output of the fractal block is  $d = 4$  convolutional layers. In a fractal block, we have  $d = 2^{c-1}$ .

### Residual connection-based fractal architectures

The residual connection can be expressed as follows where  $\oplus$  refers to feature aggregation of summation.

$$O = H(I) \oplus I \quad (4)$$

where  $H$  is a nonlinear transform and includes convolutional layers, Batch Normalization layers, and ReLU layers.

In a block of ResNet as shown in Figure 3,  $H$  is composed of two convolutional layers.

$$H_{\text{ResNet}}(I) = \text{Conv} \otimes \text{Conv}(I) \quad (5)$$

In a block of Bi-Real ResNet,  $H$  is one convolutional layer.

$$H_{\text{Bi-Real}}(I) = \text{Conv}(I) \quad (6)$$

In our residual connection-based fractal architectures, the RF-c3d4 block is shown to the middle of Figure 1, where the number of columns and the longest depth is  $c = 3$  and  $d = 4$ , respectively. All the convolutional layers are replaced with the convolutional layers with a residual connection compared with the fractal architectures of CNNs. We change the base case and the iteration rule for our residual connection-based fractal architectures. Specifically, the base case of the residual connection-based fractal architectures is as follows.

$$F_1^R(I) = \text{Conv}(I) \oplus I \quad (7)$$

Besides, we have successive fractals recursively as follows.

$$F_{C+1}^R(I) = (F_C^R \otimes F_C^R(I)) \odot (\text{Conv}(I) \oplus I) \quad (8)$$

**Discussion** The fractal architectures and residual connection-based architectures facilitate the training of full-precision DCNNs since they share the key characteristic: large nominal network depth, but effectively shorter paths for gradient propagation during training. In Bi-Real ResNet, more residual connections, where the summation is used as the operation of feature aggregation, are introduced to help the training of BCNNs. Inspired by the residual connections and fractal architectures, our residual connection-based fractal architectures combine the advantages of fractal architectures and the adoption of residual connections in one unified model to resolve the difficulty of training BCNNs.

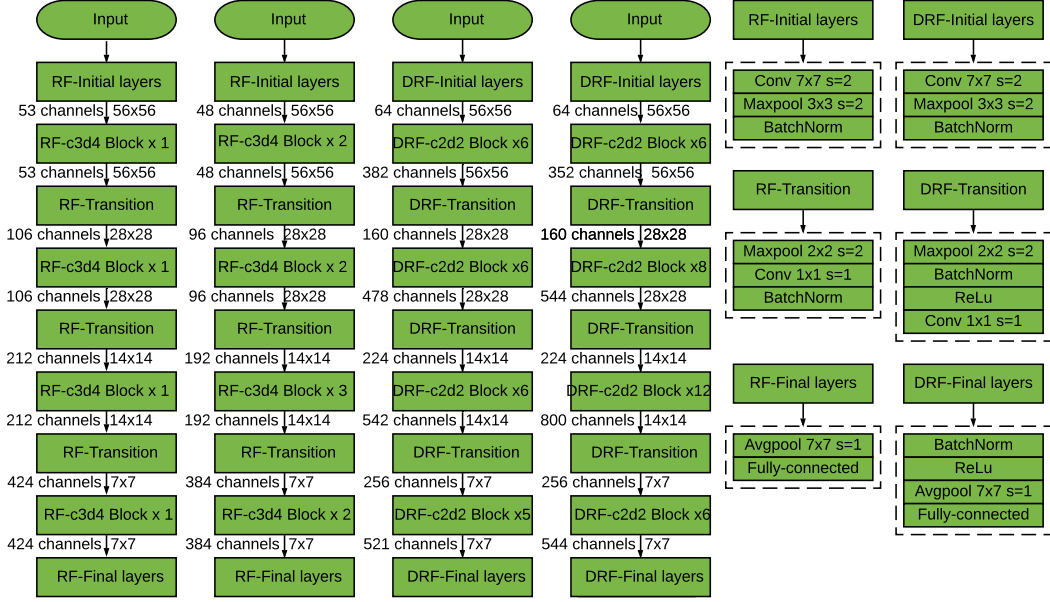


Figure 2: The building blocks and an exemplary network structure of our shortcut-based fractal architectures.

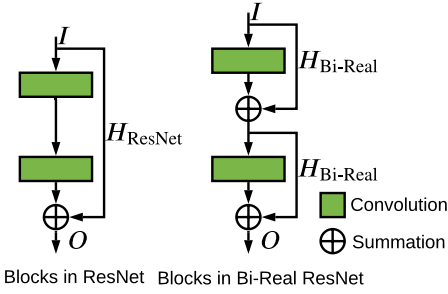


Figure 3: Blocks in ResNet and Bi-real ResNet.

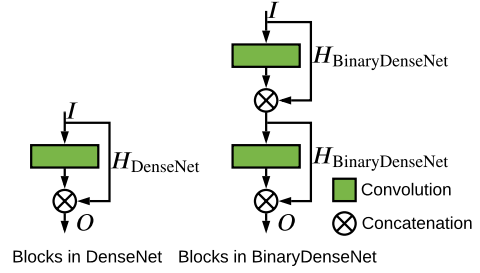


Figure 4: Blocks in DenseNet and BinaryDenseNet.

### Dense connection-based fractal architectures

The dense connection can be expressed as follows where  $\otimes$  refers to feature aggregation of concatenation.

$$O = H(I) \otimes I \quad (9)$$

where  $H$  is a nonlinear transform and includes convolutional layers, Batch Normalization layers, and ReLU layers. In a block of DenseNet as shown in Figure 4,  $H$  is composed of two convolutional layers.

$$H_{\text{DenseNet}}(I) = \text{Conv} \otimes \text{Conv}(I) \quad (10)$$

In a block of BinaryDenseNet,  $H$  is one convolutional layer.

$$H_{\text{BinaryDenseNet}}(I) = \text{Conv}(I) \quad (11)$$

In our dense connection-based fractal architectures, the DRF-c3d4 block is shown to the right of Figure 1, where the backbone, i.e., the convolutional and join layers, are the same as that in the fractal architectures. To introduce

more shortcuts, our proposed DRF-c3d4 block is a combination of dense connection, residual connection, and fractal architectures. Two characteristics need to be clarified for our dense connection-based fractal architectures. In our DRF-c3d4 block, the fractal architectures are used to produce new features maps, which will concatenate with the feature maps of all preceding convolutional layers. In the fractal architectures of our DRF-c3d4 block, all the convolution layers, where the number of output channels, are associated with the residual connections.  $F_1^D$  is the base case of our dense connection-based fractal architectures, where only one convolutional layer is used.  $F_1^D$  is calculated as follows.

$$F_1^D(I) = \text{Conv}(I) \quad (12)$$

We define the truncated fractal  $F_2^D$  as follows where three convolutional layers are used and  $F_1^R$  is the truncated fractal in our residual connection-based fractal architectures.

$$F_2^D = F_1^D \otimes F_1^R(I) \odot \text{Conv}(I) \quad (13)$$

Model	Bit-width	Top-1	Top-5	Parameters	Flops
Bi-real ResNet18(64)	$b = 32$	31.36%	11.57%	–	–
Bi-Real ResNet18(64)	$b = 1$	40.42%	18.29%	33.18Mbit	$1.64 \times 10^8$
RF-c3d4 ResNet21(53)	$b = 32$	30.91%	10.94%	–	–
RF-c3d4 ResNet21(53)	$b = 1$	37.58%	16.06%	32.63Mbit	$1.46 \times 10^8$
RF-c4d8 ResNet37(41)	$b = 32$	29.36%	10.31%	–	–
RF-c4d8 ResNet37(41)	$b = 1$	<b>37.13%</b>	<b>15.63%</b>	32.24Mbit	$1.28 \times 10^8$
RF-c5d16 ResNet69(31)	$b = 32$	28.72%	9.88%	–	–
RF-c5d16 ResNet69(31)	$b = 1$	37.66%	15.77%	32.16Mbit	$1.14 \times 10^8$
Bi-real ResNet34(64)	$b = 32$	29.24%	10.13%	–	–
Bi-Real ResNet34(64)	$b = 1$	36.74%	15.36%	43.28Mbit	$1.93 \times 10^8$
RF-c3d4 ResNet41(48)	$b = 32$	27.94%	9.47%	–	–
RF-c3d4 ResNet41(48)	$b = 1$	<b>35.62%</b>	<b>14.53%</b>	42.61Mbit	$1.64 \times 10^8$
RF-c4d8 ResNet77(35)	$b = 32$	27.61%	9.33%	–	–
RF-c4d8 ResNet77(35)	$b = 1$	36.66%	15.07%	41.53Mbit	$1.44 \times 10^8$
BinaryDenseNet51(32)	$b = 1$	38.14%	16.80%	34.80Mbit	$2.70 \times 10^8$
DRF-c2d2 DenseNet51(53)	$b = 1$	<b>36.73%</b>	<b>15.54%</b>	34.53Mbit	$2.97 \times 10^8$
BinaryDenseNet69(32)	$b = 1$	36.26%	15.24%	41.95Mbit	$2.82 \times 10^8$
DRF-c2d2 DenseNet69(48)	$b = 1$	<b>35.20%</b>	<b>14.59%</b>	41.52Mbit	$3.06 \times 10^8$

Table 1: Comparisons of binary ResNet and DenseNet variants on ImageNet.

We define the truncated fractal  $F_3^D$  as follows where seven convolutional layers are used.

$$F_3^D = F_2^D \otimes F_2^R(I) \odot \text{Conv}(I) \quad (14)$$

At the end of our dense connection-based fractal architectures, we use feature aggregation of concatenation as follows.

$$O = F_C^D \otimes I \quad (15)$$

**Discussion** Our proposed dense connection-based fractal architectures combine the advantage of the fractal architectures, residual connections, as well as dense connections in one unified model. Since the feature maps of all preceding convolutional blocks in DenseNet will be concatenated and reused, the fractal architectures are applied to produce new feature maps. Moreover, all the convolutional layers, where the number of input channels is the same as the number of output channels, adopt residual connection, so the shortcuts are used as often as possible.

### Computational complexity

We adopt the number of parameters as the metric for memory usage, and the number of Flops as the metric for computational efficiency. The number of parameters is measured as the summation of 32bits times the number of floating-point parameters and 1bit times the number of binary parameters in the model. The XNOR and Popcount bitwise operations can be executed by the current CPUs with a parallelism of 64. Therefore, the Flops is calculated by the number of floating-point multiplications plus 1/64 of the number of binary multiplication. To guarantee the fairness of the comparison, we scale the number of base channels of our SoFAR to match the computational complexity of the ResNet and DenseNet baselines.

As shown in Figure 2, we describe our SoFAR with the input images of size  $224 \times 224$ . The left two columns are the residual connection-based fractal architectures, i.e., RF-c3d4 ResNet21(53) and RF-c3d4 ResNet41(48), respectively. 21 and 41 represent the depths of our residual connection-based fractal architectures, while 53 and 48 refer to their base number of channels, which are scaled to match the computational complexity of ResNet18 and ResNet34 after binarization, respectively. Similarly, we build DRF-c2d2 DenseNet51(53) and DRF-c2d2 DenseNet69(48) to compete with DenseNet51(32) and DenseNet69(32) after binarization (Bethge et al. 2019), respectively. 51 and 69 refer to the depths of our dense connection-based fractal architectures, while 53 and 48 refer to the growth rate after scaling. We calculate the model depth with the criteria that every convolutional layer is recognized as one layer, which is different from that in (Bethge et al. 2019) (i.e., every block is recognized as a layer). To ensure consistency, binaryDenseNet28(64) and binaryDenseNet37(64) in (Bethge et al. 2019) are renamed as binaryDenseNet51(32) and binaryDenseNet69(32) in our paper. The right two columns present the composition of the initial layers, transition block, and final layers in our SoFAR.

## Experimental results

In this section, we evaluate our SoFAR on CIFAR-100 and ImageNet for the binarization of ResNet and DenseNet.

### Experimental results on ImageNet

In this section, we present the experimental results of our SoFAR on ImageNet. Compared with both binary ResNet and binary DenseNet, our SoFAR shows significant accuracy improvement for BCNNs.

Model	Bit-width	Top-1	Top-5	Parameters	Flops
Bi-real ResNet18(64)	$b = 32$	23.54%	6.55%	–	–
Bi-Real ResNet18(64)	$b = 1$	28.48%	8.65%	18.18Mbit	$1.67 \times 10^7$
RF-c3d4 ResNet21(50)	$b = 32$	22.90%	5.90%	–	–
RF-c3d4 ResNet21(50)	$b = 1$	<b>26.34%</b>	<b>7.89%</b>	18.07Mbit	$1.53 \times 10^7$
RF-c4d8 ResNet37(36)	$b = 32$	21.92%	5.87%	–	–
RF-c4d8 ResNet37(36)	$b = 1$	26.67%	7.51%	17.57Mbit	$1.42 \times 10^7$
RF-c5d16 ResNet69(26)	$b = 32$	22.38%	5.98%	–	–
RF-c5d16 ResNet69(26)	$b = 1$	26.85%	7.57%	17.63Mbit	$1.38 \times 10^7$
Bi-real ResNet34(64)	$b = 32$	21.71%	6.00%	–	–
Bi-Real ResNet34(64)	$b = 1$	27.93%	8.37%	28.28Mbit	$2.61 \times 10^7$
RF-c3d4 ResNet41(45)	$b = 32$	22.03%	5.68%	–	–
RF-c3d4 ResNet41(45)	$b = 1$	<b>25.36%</b>	<b>7.26%</b>	27.64Mbit	$2.28 \times 10^7$
RF-c4d8 ResNet77(32)	$b = 32$	21.77%	5.85%	–	–
RF-c4d8 ResNet77(32)	$b = 1$	25.57%	6.86%	27.94Mbit	$2.24 \times 10^7$
RF-c5d16 ResNet149(22)	$b = 32$	22.47%	6.19%	–	–
RF-c5d16 ResNet149(22)	$b = 1$	26.38%	7.83%	26.35Mbit	$2.08 \times 10^7$
BinaryDenseNet51(32)	$b = 1$	27.16%	7.27%	17.65Mbit	$5.13 \times 10^7$
DRF-c2d2 DenseNet51(48)	$b = 1$	<b>26.72%</b>	<b>7.51%</b>	17.51Mbit	$5.32 \times 10^7$
DRF-c3d4 DenseNet97(38)	$b = 1$	27.20%	7.74%	17.32Mbit	$5.46 \times 10^7$
BinaryDenseNet69(32)	$b = 1$	26.88%	7.52%	23.70Mbit	$5.50 \times 10^7$
DRF-c2d2 DenseNet69(44)	$b = 1$	<b>26.38%</b>	<b>7.32%</b>	23.33Mbit	$5.67 \times 10^7$
DRF-c3d4 DenseNet133(36)	$b = 1$	27.25%	7.68%	23.70Mbit	$6.02 \times 10^7$

Table 2: Comparisons of ResNet and DenseNet variants on CIFAR-100.

**ResNet variants on ImageNet** For ResNet variants, we train a full precision model as an initialization for the BCNNs. During finetuning, the weights and activations are binarized, while the downsampling convolution layer or transition block remains in full precision in BCNNs. When training the full precision model, we reorder the layers from the order of "Conv-Bn-Relu" to the order of "Conv-Relu-Bn". Regarding the training settings and data processing for ResNet variants, we train a full precision model using a momentum optimizer and a weight decay of  $1e - 4$ . We train 100 epochs in total. The learning rate starts at 0.1 and decays with a factor of 0.1 at the step of 30, 60, and 90. The Tanh function is inserted for the input activations of the convolution. During finetuning, we adopt an adam optimizer and a weight decay of 0.0. We train 50 epochs in total. The learning rate starts at  $5e - 4$  and decays at the step of 30 and 40. The Tanh function is replaced with the binarization function. We use a batch size of 256.

As shown in Table 1, we present the experimental results of our residual connection-based fractal architectures on ImageNet. RF-c4d8 ResNet37(41) indicates that there are 4 columns and 8 convolutional layers on the longest path in a block of the residual connection-based fractal architectures. All the variants of our residual connection-based fractal architectures, including RF-c3d4 ResNet21(53), RF-c4d8 ResNet37(41), and RF-c5d16 ResNet69(31), achieve significant performance improvement compared with Bi-Real ResNet18. RF-c4d8 ResNet37(41) and RF-c3d4 ResNet41(48) improve the Top-1 accuracy by 3.29% and 1.12% compared with Bi-Real ResNet18(64) and Bi-Real

ResNet34(64), respectively. Regarding the computational complexity, RF-c4d8 ResNet37(41) saves the number of parameters by 0.94Mbit and the number of Flops by  $0.36 \times 10^8$  compared with Bi-Real ResNet18(64). Similarly, the number of parameters and the number of Flops required for our proposed RF-c3d4 ResNet41(48) are 0.67Mbit and  $0.29 \times 10^8$  less than those needed for Bi-Real ResNet34(64).

**DenseNet variants on ImageNet** For DenseNet variants, we train from scratch for 100 epochs with an adam optimizer and a weight decay of 0.0. The learning rate starts at 0.002 and decreases using a cosine annealing schedule until 0.0. We use the method in (Glorot and Bengio 2010) to initialize the weights. The Relu layer is removed from the "Bn-Relu-Conv" layers.

As shown in Table 1, we present the experimental results of our dense connection-based fractal architectures on ImageNet. The Top-1 accuracy of DRF-c2d2 DenseNet51(53) and DRF-c2d2 DenseNet69(48) are 1.41% and 1.06% better than those of BinaryDenseNet51(32) and BinaryDenseNet69(32), respectively. In terms of the computational overhead, DRF-c2d2 DenseNet51(53) and DRF-c2d2 DenseNet69(48) require  $0.27 \times 10^8$  Flops and  $0.24 \times 10^8$  Flops compared with BinaryDenseNet51(32) and BinaryDenseNet69(32), respectively, while they save the number of parameters by 0.37Mbit and 0.37Mbit, respectively.

## Experimental results on CIFAR-100

In this section, we present the experimental results of binary ResNet and DenseNet variants on CIFAR-100, which shows

that our proposed SoFAR can improve the accuracy of binary ResNet and binary DenseNet with various depths.

**ResNet variants on CIFAR-100** As shown in Table 2, we present the accuracy of residual connection-based fractal architectures for binarizing ResNet18 and ResNet34. All the variants of residual connection-based fractal architectures outperform Bi-Real ResNet baselines. Compared with Bi-Real ResNet18(64) and Bi-Real ResNet34(64), the Top-1 accuracy of our RF-c3d4 ResNet21(50) and RF-c3d4 ResNet41(45) are improved by 2.14% and 2.57%, respectively. Considering the computational complexity, our RF-c3d4 ResNet21(50) use 0.11Mbit and  $0.14 \times 10^7$  Flops less than Bi-Real ResNet18(64). Our RF-c3d4 ResNet41(45) cost 0.64Mbit and  $0.33 \times 10^7$  Flops less than Bi-Real ResNet34(64).

**DenseNet variants on CIFAR-100** As shown in Table 2, we present the accuracy of dense connection-based fractal architectures for binary DenseNet51(32) and DenseNet69(32). The Top-1 accuracy of our proposed DRF-c2d2 DenseNet51(48) and DRF-c2d2 DenseNet69(44) are 0.44% and 0.50% better than those of BinaryDenseNet51(32) and BinaryDenseNet69(32), respectively. The increased number of Flops for our proposed DRF-c2d2 DenseNet51(48) and DRF-c2d2 DenseNet69(44) are  $0.19 \times 10^7$  and  $0.17 \times 10^7$ , respectively, while the decreased number of parameters for them are 0.06Mbit and 0.37Mbit, respectively, compared with BinaryDenseNet51(32) and BinaryDenseNet69(32),

### Ablation study

In the above section, we have shown the advantage of our SoFAR over the shortcut-based architectures for BCNNs, which indicate the benefits of the implicit student-teacher behavior and deep supervision of fractal architectures. In this section, we explore the role of shortcuts for our SoFAR.

Model	Bit-width	Top-1	Top-5
DRF-c2d2 DenseNet51(48)	$b = 1$	26.72%	7.51%
DF-c2d2 DenseNet51(48)	$b = 1$	27.19%	7.26%
DRF-c2d2 DenseNet69(44)	$b = 1$	26.38%	7.32%
DF-c2d2 DenseNet69(44)	$b = 1$	26.63%	7.34%
RF-c3d4 ResNet21(50)	$b = 1$	26.34%	7.89%
F-c3d4 ResNet21(50)	$b = 1$	31.82%	9.70%
RF-c3d4 ResNet41(45)	$b = 1$	25.36%	7.26%
F-c3d4 ResNet41(45)	$b = 1$	40.14%	15.19%

Table 3: Ablation study results of CIFAR-100.

The architectures of DF-c2d2 DenseNet51(48) and F-c3d4 ResNet21(50) are obtained by removing all the residual connections from DRF-c2d2 DenseNet51(48) and RF-c3d4 ResNet21(50), respectively. As shown in Table 3, the residual connections can improve the Top-1 accuracy of DF-c2d2 DenseNet51(48) and DF-c2d2 DenseNet69(44) by 0.47% and 0.25%, respectively. Similarly, the Top-1 accuracy degradation of F-c3d4 ResNet21(50) and F-c3d4

ResNet41(45) is 5.48% and 14.78% without residual connections.

Model	Top-1	Top-5
BNN ResNet18** (Courbariaux et al. 2016)	57.80%	30.80%
XNOR-Net ResNet18** (Rastegari et al. 2016)	48.80%	26.80%
TBN-ResNet18** (Wan et al. 2018)	44.40%	25.80%
Trained Bin ResNet18** (Xu and Cheung 2019)	45.80%	22.10%
CI-Net ResNet18** (Wang et al. 2019)	43.30%	19.90%
XNOR-Net++ ResNet18**	42.90%	20.10%
Bi-Real ResNet18 (Liu et al. 2018)	43.60%	20.50%
CI-Net ResNet18 (Wang et al. 2019)	40.10%	15.80%
BinaryDenseNet51(32) (Bethge et al. 2019)	39.30%	17.60%
Real-to-Bin ResNet18 (Martinez et al. 2020)	<b>34.60%</b>	<b>13.80%</b>
Bi-Real ResNet18(64)* (Liu et al. 2018)	40.42%	18.29%
BinaryDenseNet51(32)* (Bethge et al. 2019)	38.14%	16.80%
RF-c4d8 ResNet18(41)	37.13%	15.63%
DRF-c2d2 DenseNet51(53)	36.73%	15.54%
TBN-ResNet34** (Wan et al. 2018)	41.80%	19.00%
Bi-Real ResNet34 (Liu et al. 2018)	37.80%	16.10%
BinaryDenseNet69(32) (Bethge et al. 2019)	37.50%	16.10%
Bi-Real ResNet34(64)* (Liu et al. 2018)	36.74%	15.36%
BinaryDenseNet69(32)* (Bethge et al. 2019)	36.26%	15.24%
RF-c3d4 ResNet41(48)	35.62%	14.53%
DRF-c2d2 DenseNet69(48)	<b>35.20%</b>	<b>14.59%</b>
Full-precision ResNet18	30.70%	10.80%
Full-precision ResNet34	26.80%	8.60%

Table 4: Comparison with state-of-the-art methods on ImageNet. XNOR-Net++ ResNet18\*\* is from (Bulat and Tzimiropoulos 2019). \* refers to the improved baseline reproduced in our paper. \*\* indicates the downsampling layers are binarized.

### Comparison to State-of-the-Art

As shown in Table 4, we compare with state-of-the-art BCNNs on ImageNet. Except for the Real-to-Bin ResNet18 (Martinez et al. 2020), the Top-1 accuracy of our DRF-c2d2 DenseNet51(53) and DRF-c2d2 DenseNet69(48) achieve 36.73% and 35.20%, respectively, and outperforms others by a large margin. More importantly, Real-to-Bin focuses on the minimization of quantization error between the BCNNs and their full precision counterparts, while our SoFAR work towards the architecture design for BCNNs. Thus, it is reasonable to expect that the performance of Real-to-Bin can be improved further when applying our proposed architectures.

### Conclusion

In this paper, we proposed two shortcut-based fractal architectures for BCNNs: residual connection-based fractal architectures for binary ResNet, and dense connection-based fractal architectures for binary DenseNet. Benefiting from the fractal architectures and the adoption of shortcuts, our SoFAR can improve the performance of binary ResNet and binary DenseNet. Besides, we conduct experiments on classification tasks to show the advantage of our proposal. Under a given computational complexity budget, our proposed SoFAR achieves significantly better accuracy than current state-of-the-art BCNNs.

## References

- Ba, J.; and Caruana, R. 2014. Do deep nets really need to be deep? In *Advances in neural information processing systems*, 2654–2662.
- Bengio, Y.; Léonard, N.; and Courville, A. 2013. Estimating or propagating gradients through stochastic neurons for conditional computation. *arXiv preprint arXiv:1308.3432*.
- Bethge, J.; Yang, H.; Bornstein, M.; and Meinel, C. 2019. BinaryDenseNet: Developing an Architecture for Binary Neural Networks. In *Proceedings of the IEEE International Conference on Computer Vision Workshops*, 0–0.
- Bulat, A.; and Tzimiropoulos, G. 2019. XNOR-Net++: Improved Binary Neural Networks. *arXiv arXiv-1909*.
- Cai, Y.; Yao, Z.; Dong, Z.; Gholami, A.; Mahoney, M. W.; and Keutzer, K. 2020. Zeroq: A novel zero shot quantization framework. In *Proceedings of the IEEE/CVF Conference on Computer Vision and Pattern Recognition*, 13169–13178.
- Chen, L.-C.; Papandreou, G.; Schroff, F.; and Adam, H. 2017. Rethinking atrous convolution for semantic image segmentation. *arXiv preprint arXiv:1706.05587*.
- Courbariaux, M.; Hubara, I.; Soudry, D.; El-Yaniv, R.; and Bengio, Y. 2016. Binarized neural networks: Training deep neural networks with weights and activations constrained to +1 or -1. *arXiv preprint arXiv:1602.02830*.
- Darabi, S.; Belbahri, M.; Courbariaux, M.; and Nia, V. P. 2018. Bnn+: Improved binary network training. *arXiv preprint arXiv:1812.11800*.
- Ding, R.; Chin, T.-W.; Liu, Z.; and Marculescu, D. 2019. Regularizing activation distribution for training binarized deep networks. In *Proceedings of the IEEE Conference on Computer Vision and Pattern Recognition*, 11408–11417.
- Dong, Z.; Yao, Z.; Gholami, A.; Mahoney, M. W.; and Keutzer, K. 2019. Hawq: Hessian aware quantization of neural networks with mixed-precision. In *Proceedings of the IEEE International Conference on Computer Vision*, 293–302.
- Glorot, X.; and Bengio, Y. 2010. Understanding the difficulty of training deep feedforward neural networks. In *Proceedings of the thirteenth international conference on artificial intelligence and statistics*, 249–256.
- Gong, R.; Liu, X.; Jiang, S.; Li, T.; Hu, P.; Lin, J.; Yu, F.; and Yan, J. 2019. Differentiable soft quantization: Bridging full-precision and low-bit neural networks. In *Proceedings of the IEEE International Conference on Computer Vision*, 4852–4861.
- He, K.; Zhang, X.; Ren, S.; and Sun, J. 2016. Deep residual learning for image recognition. In *Proceedings of the IEEE conference on computer vision and pattern recognition*, 770–778.
- He, Y.; Ding, Y.; Liu, P.; Zhu, L.; Zhang, H.; and Yang, Y. 2020. Learning Filter Pruning Criteria for Deep Convolutional Neural Networks Acceleration. In *IEEE/CVF Conference on Computer Vision and Pattern Recognition (CVPR)*.
- He, Z.; and Fan, D. 2019. Simultaneously optimizing weight and quantizer of ternary neural network using truncated gaussian approximation. In *Proceedings of the IEEE Conference on Computer Vision and Pattern Recognition*, 11438–11446.
- Hou, L.; Yao, Q.; and Kwok, J. T. 2016. Loss-aware binarization of deep networks. *arXiv preprint arXiv:1611.01600*.
- Howard, A.; Sandler, M.; Chu, G.; Chen, L.-C.; Chen, B.; Tan, M.; Wang, W.; Zhu, Y.; Pang, R.; Vasudevan, V.; et al. 2019. Searching for mobilenetv3. In *Proceedings of the IEEE International Conference on Computer Vision*, 1314–1324.
- Huang, G.; Liu, Z.; Van Der Maaten, L.; and Weinberger, K. Q. 2017. Densely connected convolutional networks. In *Proceedings of the IEEE conference on computer vision and pattern recognition*, 4700–4708.
- Iandola, F. N.; Han, S.; Moskewicz, M. W.; Ashraf, K.; Dally, W. J.; and Keutzer, K. 2016. SqueezeNet: AlexNet-level accuracy with 50x fewer parameters and 0.5 MB model size. *arXiv preprint arXiv:1602.07360*.
- Jung, S.; Son, C.; Lee, S.; Son, J.; Han, J.-J.; Kwak, Y.; Hwang, S. J.; and Choi, C. 2019. Learning to quantize deep networks by optimizing quantization intervals with task loss. In *Proceedings of the IEEE Conference on Computer Vision and Pattern Recognition*, 4350–4359.
- Khan, A.; Sohail, A.; Zahoor, U.; and Qureshi, A. S. 2020. A survey of the recent architectures of deep convolutional neural networks. *Artificial Intelligence Review* 1–62.
- Lahoud, F.; Achanta, R.; Márquez-Neila, P.; and Süsstrunk, S. 2019. Self-binarizing networks. *arXiv preprint arXiv:1902.00730*.
- Larsson, G.; Maire, M.; and Shakhnarovich, G. 2016. Fractalnet: Ultra-deep neural networks without residuals. *arXiv preprint arXiv:1605.07648*.
- Lee, C.-Y.; Xie, S.; Gallagher, P.; Zhang, Z.; and Tu, Z. 2015. Deeply-supervised nets. In *Artificial intelligence and statistics*, 562–570.
- Li, C.; Peng, J.; Yuan, L.; Wang, G.; Liang, X.; Lin, L.; and Chang, X. 2020a. Block-wisely Supervised Neural Architecture Search with Knowledge Distillation. In *Proceedings of the IEEE/CVF Conference on Computer Vision and Pattern Recognition*, 1989–1998.
- Li, Y.; Wang, W.; Bai, H.; Gong, R.; Dong, X.; and Yu, F. 2020b. Efficient Bitwidth Search for Practical Mixed Precision Neural Network. *arXiv preprint arXiv:2003.07577*.
- Liu, L.; Ouyang, W.; Wang, X.; Fieguth, P.; Chen, J.; Liu, X.; and Pietikäinen, M. 2020. Deep learning for generic object detection: A survey. *International journal of computer vision* 128(2): 261–318.
- Liu, Z.; Wu, B.; Luo, W.; Yang, X.; Liu, W.; and Cheng, K.-T. 2018. Bi-real net: Enhancing the performance of 1-bit cnns with improved representational capability and advanced training algorithm. In *Proceedings of the European conference on computer vision (ECCV)*, 722–737.



- Ma, N.; Zhang, X.; Zheng, H.-T.; and Sun, J. 2018. Shufflenet v2: Practical guidelines for efficient cnn architecture design. In *Proceedings of the European conference on computer vision (ECCV)*, 116–131.
- Martinez, B.; Yang, J.; Bulat, A.; and Tzimiropoulos, G. 2020. Training binary neural networks with real-to-binary convolutions. *arXiv preprint arXiv:2003.11535* .
- Mishra, A.; and Marr, D. 2017. Apprentice: Using knowledge distillation techniques to improve low-precision network accuracy. *arXiv preprint arXiv:1711.05852* .
- Mishra, A.; Nurvitadhi, E.; Cook, J. J.; and Marr, D. 2017. WRPN: wide reduced-precision networks. *arXiv preprint arXiv:1709.01134* .
- Qin, H.; Gong, R.; Liu, X.; Shen, M.; Wei, Z.; Yu, F.; and Song, J. 2020. Forward and Backward Information Retention for Accurate Binary Neural Networks. In *Proceedings of the IEEE/CVF Conference on Computer Vision and Pattern Recognition*, 2250–2259.
- Rastegari, M.; Ordonez, V.; Redmon, J.; and Farhadi, A. 2016. Xnor-net: Imagenet classification using binary convolutional neural networks. In *European conference on computer vision*, 525–542. Springer.
- Romero, A.; Ballas, N.; Kahou, S. E.; Chassang, A.; Gatta, C.; and Bengio, Y. 2014. Fitnets: Hints for thin deep nets. *arXiv preprint arXiv:1412.6550* .
- Shen, M.; Han, K.; Xu, C.; and Wang, Y. 2019. Searching for accurate binary neural architectures. In *Proceedings of the IEEE International Conference on Computer Vision Workshops*, 0–0.
- Szegedy, C.; Liu, W.; Jia, Y.; Sermanet, P.; Reed, S.; Anguelov, D.; Erhan, D.; Vanhoucke, V.; and Rabinovich, A. 2015. Going deeper with convolutions. In *Proceedings of the IEEE conference on computer vision and pattern recognition*, 1–9.
- Tan, M.; Chen, B.; Pang, R.; Vasudevan, V.; Sandler, M.; Howard, A.; and Le, Q. V. 2019. Mnasnet: Platform-aware neural architecture search for mobile. In *Proceedings of the IEEE Conference on Computer Vision and Pattern Recognition*, 2820–2828.
- Verelst, T.; and Tuytelaars, T. 2020. Dynamic Convolutions: Exploiting Spatial Sparsity for Faster Inference. In *IEEE/CVF Conference on Computer Vision and Pattern Recognition (CVPR)*.
- Wan, D.; Shen, F.; Liu, L.; Zhu, F.; Qin, J.; Shao, L.; and Tao Shen, H. 2018. Tbn: Convolutional neural network with ternary inputs and binary weights. In *Proceedings of the European Conference on Computer Vision (ECCV)*, 315–332.
- Wang, T.; Wang, K.; Cai, H.; Lin, J.; Liu, Z.; Wang, H.; Lin, Y.; and Han, S. 2020. APQ: Joint Search for Network Architecture, Pruning and Quantization Policy. In *Proceedings of the IEEE/CVF Conference on Computer Vision and Pattern Recognition*, 2078–2087.
- Wang, Z.; Lu, J.; Tao, C.; Zhou, J.; and Tian, Q. 2019. Learning channel-wise interactions for binary convolutional neural networks. In *Proceedings of the IEEE Conference on Computer Vision and Pattern Recognition*, 568–577.
- Wu, B.; Dai, X.; Zhang, P.; Wang, Y.; Sun, F.; Wu, Y.; Tian, Y.; Vajda, P.; Jia, Y.; and Keutzer, K. 2019. Fbnet: Hardware-aware efficient convnet design via differentiable neural architecture search. In *Proceedings of the IEEE Conference on Computer Vision and Pattern Recognition*, 10734–10742.
- Wu, B.; Wan, A.; Yue, X.; Jin, P.; Zhao, S.; Golmant, N.; Gholaminejad, A.; Gonzalez, J.; and Keutzer, K. 2018a. Shift: A zero flop, zero parameter alternative to spatial convolutions. In *Proceedings of the IEEE Conference on Computer Vision and Pattern Recognition*, 9127–9135.
- Wu, B.; Wang, Y.; Zhang, P.; Tian, Y.; Vajda, P.; and Keutzer, K. 2018b. Mixed precision quantization of convnets via differentiable neural architecture search. *arXiv preprint arXiv:1812.00090* .
- Xu, Z.; and Cheung, R. C. 2019. Accurate and compact convolutional neural networks with trained binarization. *arXiv preprint arXiv:1909.11366* .
- Yang, J.; Shen, X.; Xing, J.; Tian, X.; Li, H.; Deng, B.; Huang, J.; and Hua, X.-s. 2019. Quantization networks. In *Proceedings of the IEEE Conference on Computer Vision and Pattern Recognition*, 7308–7316.
- Zhang, Z.; Li, J.; Shao, W.; Peng, Z.; Zhang, R.; Wang, X.; and Luo, P. 2019. Differentiable learning-to-group channels via groupable convolutional neural networks. In *Proceedings of the IEEE International Conference on Computer Vision*, 3542–3551.
- Zhou, S.; Wu, Y.; Ni, Z.; Zhou, X.; Wen, H.; and Zou, Y. 2016. Dorefa-net: Training low bitwidth convolutional neural networks with low bitwidth gradients. *arXiv preprint arXiv:1606.06160* .
- Zhu, B.; Al-Ars, Z.; and Hofstee, P. 2020. NASB: Neural Architecture Search for Binary Convolutional Neural Networks. *arXiv preprint arXiv:2008.03515* .
- Zhu, B.; Al-Ars, Z.; and Pan, W. 2020. Towards Lossless Binary Convolutional Neural Networks Using Piecewise Approximation.
- Zhuang, B.; Shen, C.; Tan, M.; Liu, L.; and Reid, I. 2019. Structured binary neural networks for accurate image classification and semantic segmentation. In *Proceedings of the IEEE Conference on Computer Vision and Pattern Recognition*, 413–422.